Structural studies of disordered materials using high-energy x-ray diffraction from ambient to extreme conditions

2007 J. Phys.: Condens. Matter 19 506101

(http://iopscience.iop.org/0953-8984/19/50/506101)

IOP PUBLISHING JOURNAL OF PHYSICS: CONDENSED MATTER

J. Phys.: Condens. Matter **19** (2007) 506101 (15pp) doi:10.1088/0953-8984/19/50/506101

Structural studies of disordered materials using high-energy x-ray diffraction from ambient to extreme conditions

Shinji Kohara[1,2], Masayoshi Itou[1], Kentaro Suzuya[3], Yasuhiro Inamura[3], Yoshiharu Sakurai[1], Yasuo Ohishi[1,2] and Masaki Takata[1,2,4,5]

[1] Japan Synchrotron Radiation Research Institute (SPring-8/JASRI), 1-1-1 Kouto, Sayo, Hyogo 679-5198, Japan
[2] CREST-JST, Japan
[3] Japan Atomic Energy Agency (J-PARC/JAEA), Tokai, Naka, Ibaraki 319-1195, Japan
[4] SPring-8/RIKEN, 1-1-1 Kouto, Sayo, Hyogo 679-5148, Japan
[5] Department of Advanced Materials Science, School of Frontier Sciences, The University of Tokyo, 5-1-5 Kashiwanoha, Kashiwa, Chiba 277-8561, Japan

Received 30 April 2007, in final form 18 September 2007
Published 8 November 2007
Online at stacks.iop.org/JPhysCM/19/506101

Abstract

High-energy x-rays from a synchrotron radiation source allow us to obtain high-quality diffraction data for disordered materials from ambient to extreme conditions, which is necessary for revealing the detailed structures of glass, liquid and amorphous materials. We introduced high-energy x-ray diffraction beamlines and a dedicated diffractometer for glass, liquid and amorphous materials at SPring-8 and report the recent developments of ancillary equipment. Furthermore, the structures of liquid and amorphous materials determined from the high-energy x-ray diffraction data obtained at SPring-8 are discussed.

1. Introduction

The diffraction method yields accurate bulk average structural information or atomic positions of crystalline and disordered materials. Typically, in the structural analysis of disordered materials, x-ray and neutron diffraction can be used to directly measure local and intermediate-range or nanoscale structures, atomic bond lengths and coordination numbers by the Fourier transformation of the total structure factor $S(Q)$ ($Q = (4\pi/\lambda)\sin\theta$ with 2θ the scattering angle and λ the photon wavelength) to a real space function using the following equation:

$$g(r) = 1 + \frac{1}{2\pi^2\rho r}\int_{Q_{\min}}^{Q_{\max}} Q[S(Q) - 1]\sin(Qr)\,\mathrm{d}Q. \quad (1)$$

To obtain real space information with a sufficient resolution it is necessary to measure $S(Q)$ up to the higher Q region since higher resolution in real space is achieved with larger $Q_{\max}$.

Neutron diffraction has widely been used for structural studies of disordered materials, particularly when using the isotopic substitution technique, since spallation sources make it

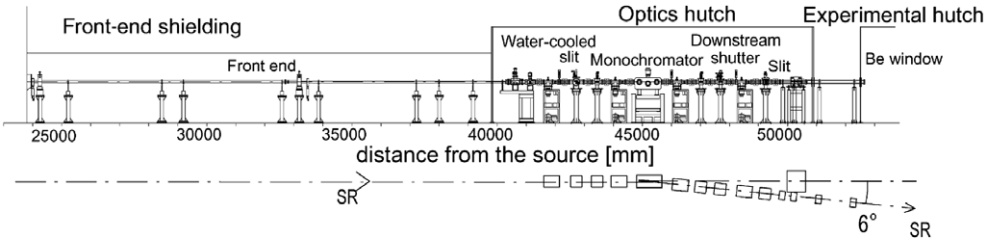

Figure 1. A schematic drawing of the beamline.

possible to obtain high-Q data with the time of flight technique. On the other hand, x-rays from conventional x-ray sources can provide low-energy x-rays with an insufficient beam flux. Therefore an accessible maximum Q is very limited [1] and the quality and amount of data are not as good as for neutron data. However, with the arrival of the latest generation of synchrotron sources and the introduction of advanced insertion devices (wigglers and undulators), the use of high-energy ($E \geqslant 50$ keV) x-rays has become feasible [2]. Diffraction experiments using high-energy x-rays have the following advantages:

(i) Although x-ray diffraction data typically suffer from a significant decrease in coherent scattering cross section, high-energy x-rays provide us high-Q data with small scattering angles, which suppress the energy- and 2θ-dependent correction terms (particularly the absorption correction term).
(ii) High-energy x-rays expand the capability of transmission geometry due to high penetration power. We can use a millimeter-thickness container for the powder and liquid samples containing heavy elements.
(iii) Highly collimated x-rays with high flux density allow us to perform experiments in extreme conditions, including high temperatures and high pressures. Small scattering angles suppress the window area of the furnace and the high-pressure vessel.
(iv) High-flux x-rays are suitable for time-resolved diffraction experiments when combined with an area detector.

Since x-rays and neutrons are scattered by electrons and nuclei, respectively, a combination of x-ray and neutron diffraction provides diffraction data with different contrasts. Thus, a combination of x-ray and neutron diffraction is a powerful tool for probing the complicated structures of disordered materials. Details of the recent progress in both techniques involving high-energy x-rays and neutrons, as well as in data analysis and computer simulation, have been reviewed by Fisher *et al* [3] and described in detail by Egami and Billinge [4].

In this article, we introduce the facility for high-energy x-ray diffraction experiments with disordered materials at SPring-8: high-energy x-ray beamlines, a diffractometer dedicated to glass, liquid and amorphous materials. We report the recent developments of ancillary equipment (automatic sample changer, conventional high-temperature furnace, aerodynamic levitation furnace and electrostatic levitation furnace) for experiments under conventional and extreme conditions, and recent scientific results.

2. Instrumentation

2.1. High-energy x-ray diffraction beamline BL04B2

Since the first high-energy x-ray diffraction experiment on amorphous silica was reported by Poulsen and Neuefeind *et al* in 1995 [1, 2], a structural study of disordered materials

Table 1. Available photon energy, energy resolution, photon flux, and beam size of BL04B2.

Energy	Si(111): 37.8 keV 113.3 keV (third harmonic reflection) Si(220): 61.7 keV
Energy resolution	$\Delta E/E = 10^{-3}$ at 15 m from the monochromator (at incident beam size: 0.2 (H) × 4 (W) mm^2)
Photon flux	37.8 keV Flat: 2.2×10^{10} (photons/sec/1 × 1 mm^2 at 100 mA) Bent: 7.1×10^{11} 61.7 keV Flat: 3.4×10^{9} Bent: 9.2×10^{10}
Beam size	37.8 keV: 0.220 mm 61.7 keV: 0.375 mm (at incident beam size: 0.2 (H) × 4 (W) mm^2)

using high-energy x-ray diffraction has become feasible and popular over the past 10 years. Nevertheless, the number of dedicated beamlines for disordered materials, where high-energy x-ray diffraction experiments can be performed, is still limited.

One of the beamlines that enables us to perform such structural studies of disordered materials at SPring-8 is the high-energy x-ray diffraction beamline BL04B2 [5]. The schematic layout of the beamline is shown in figure 1. The light source of BL04B2 is a bending magnet whose critical energy is 28.9 keV. Synchrotron radiation from the bending magnet is guided through a standard front-end into the experimental hall. The front-end section is extended by 16 m in the narrow space of the experimental hall and covered by front-end shielding. The horizontal divergence of the beam is limited to 0.73 mrad by a fixed mask. Part of the transport channel, which consists of standard components and a bent-crystal monochromator, is accommodated in the optics hutch. A Pb-shielded flight path connects the optics hutch with the experimental hutch. The end of the flight path is terminated with a 0.25 mm thick Be window.

To carry out experiments using high-energy and focused x-rays in this beamline we adopt a single-bounce, bent-crystal monochromator which deflects the beam horizontally. The Bragg angle is fixed at 3°, so that we can discretely change the energy by changing reflection net planes. The monochromator can be mounted two Si crystals, which facilitates energy switching by vertical translation. The Si(111) (37.8 keV) and Si(220) (61.7 keV) crystals are mounted on a water-cooled crystal holder with an In sheet in order to obtain a sufficient thermal contact. The mechanism of this system is similar to that of standard mirror supports used for the horizontal focusing of x-rays from an undulator beamline. The monochromator with two crystals was installed at 46 m from the light source. The adjustable bending radius (320–430 m) enables us to adjust the focal position at 10–15 m (distance from the monochromator) in the experimental hutch. The peak flux density of an optimally bent crystal was 35 times higher than that of a flat crystal [5]. One of the advantages of the single-bounce, bent-crystal monochromator is the negligible drift of monochromatized x-rays, which is important for the accurate measurement of diffraction patterns of disordered materials up to the high-Q region. This property is enhanced when combined with the top-up operation of the storage ring [6], which provides a constant heat load to the monochromator crystal.

The horizontal beam divergence of the monochromator measured using the Si(111) analyzer crystal positioned at 15 m from the monochromator was 50 arcsec [5],

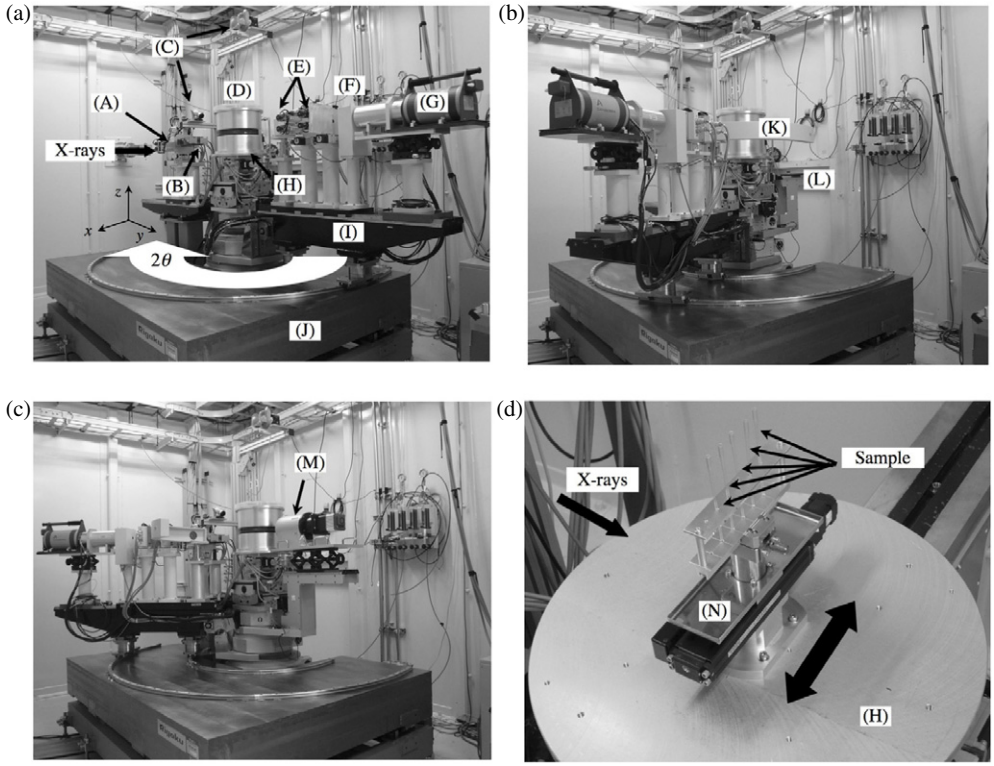

Figure 2. Photographs of the two-axis diffractometer for disordered materials. (a) Step scan mode with a Ge detector ($2\theta = 0$). (b) Step-scan mode with a Ge detector ($2\theta = 60$, the beam stop can be seen). (c) Fast diffraction measurement mode with an x-ray image intensifier. (d) Automatic sample changer for cylindrical sample. (A) 4D incident slit, (B) ionization chamber, (C) sample monitor camera, (D) vacuum chamber, (E) 2D receiving slits (700 mm (upstream) and 850 mm (downstream) from the sample), (F) fully automatic attenuator, (G) intrinsic Ge detector, (H) θ stage, (I) 2θ main arm, (J) table, (K) incident beam stop, (L) 2θ sub arm, (M) x-ray image intensifier, (N) fully automatic sample changer.

which agrees with that expected from geometrical consideration (incident beam size 0.2 mm (H) $\times$ 4 mm (W)). The energy resolution,

$$\Delta E/E \sim |(\sigma p - \sigma q)^2 + \omega^2|^{1/2} \cot\theta_{\mathrm{B}}, \tag{2}$$

can be estimated from the beam divergence, which depends on the slit width and the bending radius, as

$$\Delta E/E = \cot\theta_{\mathrm{B}} \sim 20l/L, \tag{3}$$

where l is the horizontal slit width and L is the distance from the monochromator to the focal position. The energy resolution under the above conditions was estimated to be about 5×10^{-3} [5]. The available incident energy of x-rays, energy resolution, photon flux and beam size are summarized in table 1.

2.2. Two-axis diffractometer for disordered materials

We have developed a two-axis diffractometer [7] dedicated for disordered materials. A photograph of the two-axis diffractometer for glass, liquid and amorphous materials is shown

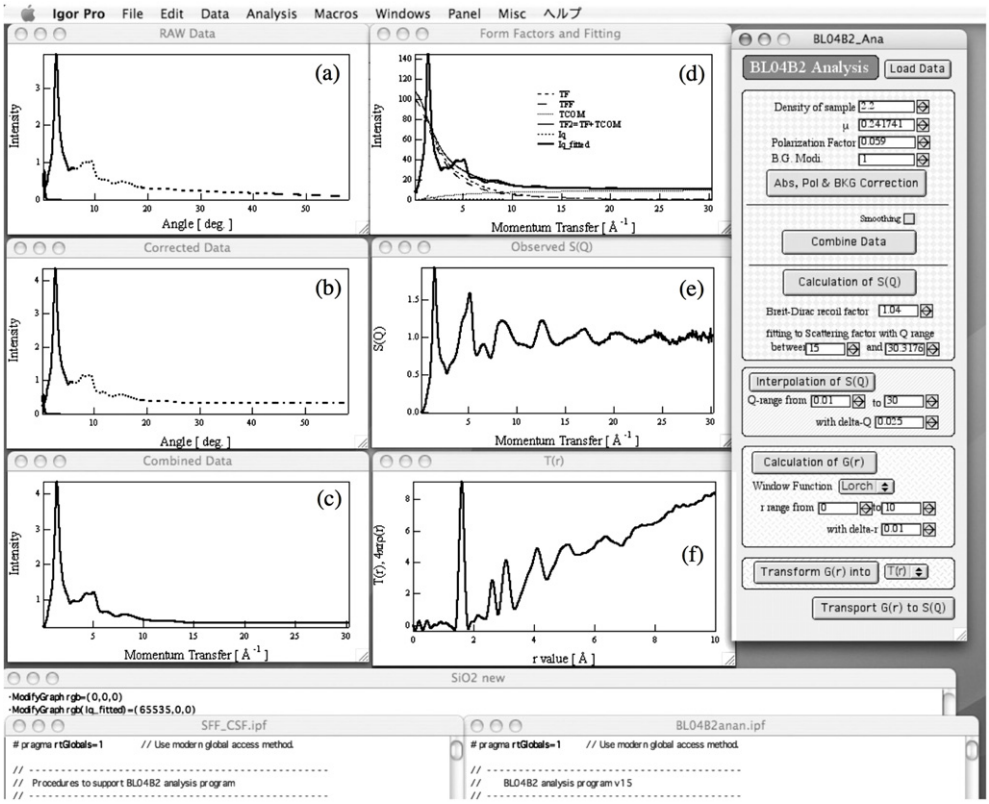

Figure 3. Main graphical user interface of data analysis software.

in figure 2. The diffractometer was designed with a horizontal scattering plane for easier use of heavy equipment, although the horizontal scattering plane includes a significant polarization factor in the large scattering angle region. In high-energy x-ray diffraction, however, the experiment can be performed with small scattering angles, at which the effect of the polarization factor is not very significant.

The accessible angular region of the 2θ main arm (I in figure 2(a)) spans from $-10°$ to $150°$ with a minimum scan step of $0.0001°$. The 2θ sub arm (L in figure 2(b)), which is designed for use of the area detector, has an accessible angular region spanning from $-120°$ to $10°$ with a minimum scan step of $0.001°$. The accessible angular domain of the θ stage (H in figures 2(a) and (d)) spans from $-180°$ to $180°$ with a minimum scan step of $0.001°$. Furthermore, the θ stage moves freely in five ways: translations in the X (± 10 mm), Y (± 10 mm) and Z (± 10 mm) directions, and the R_x ($\pm 3°$) and R_y ($\pm 3°$) rotations. The entire diffractometer is mounted on a heavy-duty table (J in figure 2(a)) which moves in the X_t (± 15 mm) direction. All movements are driven by stepping motors.

The direct beam stop is a very important component for reducing air scattering in measurements around the small angle region. As can be seen from figure 2(b), the incident beam stop (K in figure 2(b)) is mounted on the 2θ main arm, so that the beam stop and the 2θ main arm can move together. This component also effectively reduces the air scattering background around the small angle region more than the incident beam stop mounted on the table of the diffractometer.

As mentioned above, the diffractometer has two 2θ arms, one is for normal step-scan measurement using an intrinsic Ge detector and the other is for fast measurement using an area detector. The advantage of step-scan measurement is that it provides us data of good quality, since the contribution of the background is extremely small due to the receiving slits (see figure 7(a)) and Ge can discriminate unfavorable scatterings, e.g. fluorescence from heavy atoms and incoherent scattering in a high-Q region, although it requires a long time, between 2 and 12 h (depending on $Q_{\max}$ and the amount of sample). On the other hand, an area detector (for example, an x-ray image intensifier enables us to measure a diffraction pattern within a 30 ms shot) is extremely useful for fast measurement, but the contribution of the background is large and the area detector does not allow sufficient energy discrimination. The advantage of our diffractometer is that we can switch the step-scan mode and the fast measurement mode without any alignment so that we can conveniently perform both measurements according to the scientific objective.

The typical beam size at the sample position is 2.5 mm (H) $\times$ 0.5 mm (W) and we can also reduce the size for a small amount of the sample. The typical widths of the receiving slits are 0.8 mm (upstream) and 0.5 mm (downstream) but the slit size can be changed according to the user's request. Thus, by the use of the diffractometer, one can obtain a reliable structure factor in a wide Q range with a small amount of sample $\sim$5 mg.

The two-axis diffractometer is controlled by software developed employing C language on a Linux operating system. We can collect not only discriminated counts from a Ge detector via the GPIB interface, but also the energy spectrum of the detector integrated with a multichannel analyzer via the Ethernet. The energy spectra from the multichannel analyzer are very important for analytically eliminating the contribution of incoherent scattering at a high Q. To obtain a higher counting rate with a small dead time, a YAP(Ce) scintillation counter can be used when a high energy resolution is not necessary.

Ensuring the accuracy of data collection techniques in research on disordered materials is important for obtaining excellent quantitative results. In SPring-8, the data analysis software was developed using IGOR (WaveMetrics, Inc., Lake Oswego, OR, USA). The main graphical user interface of the analysis software and a typical input file are shown in figure 3. The data file names, sample composition, geometric parameters, atomic density, absorption coefficients and incident photon energy are given in the input file, and then the software system carries out data reduction (figure 3(a)), data corrections (background, polarization and absorption corrections, figure 3(b)), the combination of separate runs (figure 3(c)), data normalization to the structure factor (figures 3(d) and (e)) and Fourier transformation (figure 3(f)). This software is user-friendly and easy to operate for first time users.

In typical experiments using a step-scan method at room temperature, the automatic sample changer is the most useful ancillary equipment to users. The fully automatic sample changer with an x-translation stage (figure 2(d)) allows us to perform automatic measurements for up to five cylindrical or flat-plate shaped samples with/without a container. A conventional high-temperature furnace dedicated for the two-axis diffractometer up to 1100 °C is another useful ancillary item. A typical sample container is a Pyrex or silica tube of 2 mm ID $\times$ 0.2 mm t $\times$ 65 mm length.

Recently levitation furnaces have been developed to study the structures of containerless liquids and undercooled liquids, which is key to understanding glass formation. The use of containerless techniques such as electromagnetic [8–10], aerodynamic [11–14] and electrostatic [15–17] levitations allows us to study highly reactive melts for a wide range of temperatures and the metastable phase including deeply undercooled liquids. Accordingly various levitation furnaces have already been developed at synchrotron and neutron sources. The aerodynamic and the electrostatic levitation furnaces have been developed, respectively,

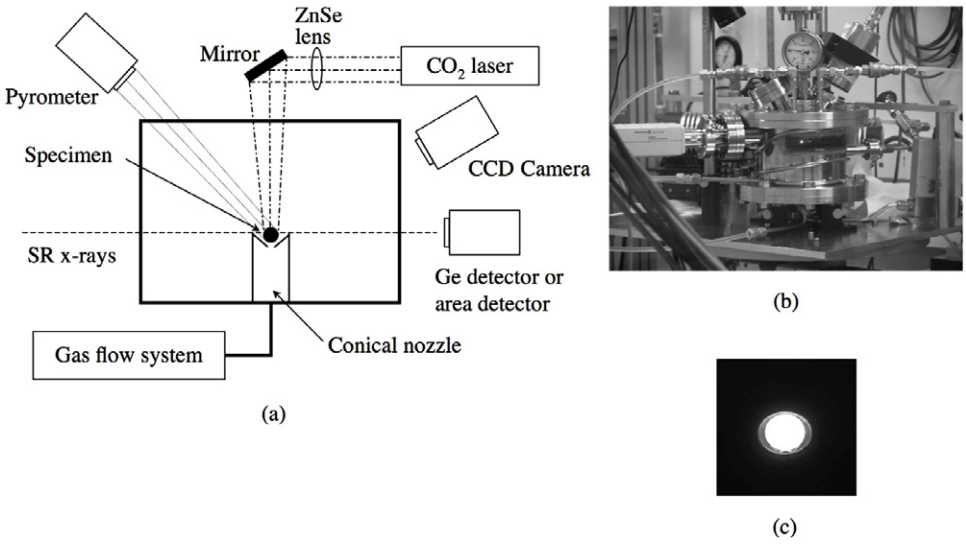

Figure 4. Schematic drawing of an aerodynamic levitation furnace (a), and photographs of the aerodynamic levitation furnace (b) and levitated specimen (c) (liquid $Zr_{70}Cu_{30}$ at 1453 K) [18].

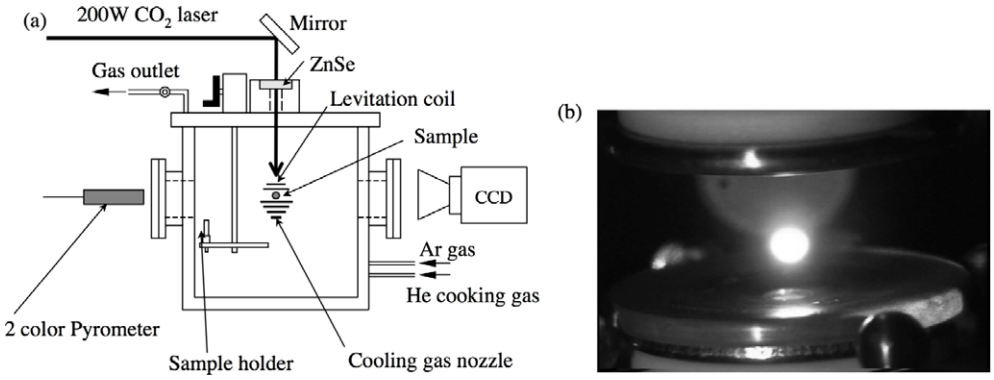

Figure 5. Schematic drawing of an electrostatic levitation furnace (a) and photograph of a levitated specimen (b) (liquid Zr at 2125 K) [19].

by Mizuno *et al* [18] and Masaki *et al* [19] for BL04B2. An electrostatic levitation furnace is also available at the high-energy Compton scattering beamline BL08W [20] and at the inelastic x-ray scattering beamline BL35XU [21, 22]. The schematic views with the photographs for the furnaces of aerodynamic and electrostatic levitations are shown in figures 4 and 5, respectively. Since the position of the levitated liquid sample in both furnaces is stable, we have succeeded in measuring a reliable structure factor for the levitated liquid up to $Q \sim 20$ Å^{-1} with sufficient statistics. Using these systems both hour-long (up to 2 h) and fast (30 ms) containerless measurements are achievable with a Ge detector (step-scan) and an image intensifier, respectively.

2.3. Image plate diffractometer for high-energy x-ray diffraction of disordered materials under high pressure

A diffractometer with an image plate was designed for high-energy x-ray diffraction experiments under high pressures using a DAC (diamond anvil cell). A schematic view and photograph of this diffractometer are shown in figure 6. A flat image plate detector (automatic IP reading system, Rigaku/R-AXIS IV, area 30×30 cm^2 and pixel size 0.10 mm) detector and optical components are aligned on the 2θ arm. The camera distance can be varied from 230 to 600 cm in order to optimize the 2θ resolution and detectable region. The diffractometer consists of various optical devices, namely, an ionization chamber for monitoring beam intensity, a four-blade slit, attenuators, a beam shutter, and an incident beam stop. The blades of the slit, the beam shutter and the beam stop are made from Ta or Pb metal with a thickness of 5 mm. The shape of the monochromatized incident beam is usually trimmed by the four-blade slit to a size of 0.01–1.0 mm^2. To reduce the beam size or to eliminate an unfavorable diffraction from the gasket material surrounding the sample chamber in the DAC, a collimator with a diameter of less than 0.04 mm is used. To oscillate the single crystal or polycrystalline specimen, X–Y–Z stages for the DAC are mounted on a ω-stage. On-line IP reading and data collection procedures are controlled by a PC with Microsoft Windows.

2.4. High-energy x-ray diffraction using 176 keV x-rays

As we introduced above, diffraction experiments at BL04B2 are well developed. However, in the case of the bending magnet beamline, the photon flux at the energy greater than 100 keV is insufficient, particularly for the sample containing heavy elements, because of large absorption coefficients. Accordingly, high-energy x-rays from an insertion device are necessary in such a case. In SPring-8, the only wiggler beamline, BL08W [20], is available for such a purpose, because the wiggler can give us higher energy x-rays with a sufficient photon flux. A two-axis diffractometer can be optionally installed at BL08W, which is equipped with an elliptical multipole wiggler with a critical energy of 42.7 keV at a 25.5 mm gap [23]. The white x-rays emitted from the wiggler are monochromatized and focused by an asymmetric Johann-type monochromator [24]. The Si(620) reflection is used with an asymmetry angle of $\sim 1^\circ$. The energy of the monochromatized x-rays is 175.7 keV with the energy resolution $\Delta E/E \sim 2 \times 10^{-3}$ keV. The beam size at the sample is 1.5 mm (H) $\times$ 0.5 mm (W). The overall experimental arrangement in BL08W is very similar to that in BL04B2. The spectrometer employed a Ge detector which is placed on the 2θ arm at a distance of 650 mm from the central axis. The scattered x-rays from the sample are collected by the Ge detector integrated with a digital signal processor (DSP)-based multichannel analyzer system. To suppress the background from air scattering around the sample, two slits of width 0.5 mm are installed between the sample and the detector. Furthermore, a sample chamber filled with He gas is also installed to suppress the air scattering, too. An ionization chamber is placed upstream of the sample to monitor the intensity of incident x-rays.

3. Results

3.1. Typical diffraction data

Amorphous silica is an archetypal oxide glass, which has been a subject of diffraction study [25, 26]. Amorphous silica is also a very important standard material. The x-ray diffraction pattern together with background data is shown in figure 7(a). As can be observed in the inset figure in figure 7(a), we succeeded in suppressing the background due to the

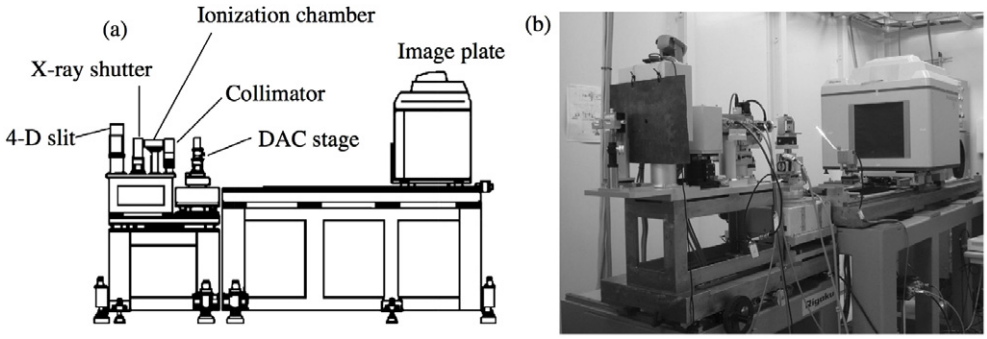

Figure 6. Schematic drawing (a) and photograph (b) of the image plate diffractometer for high-energy x-rays.

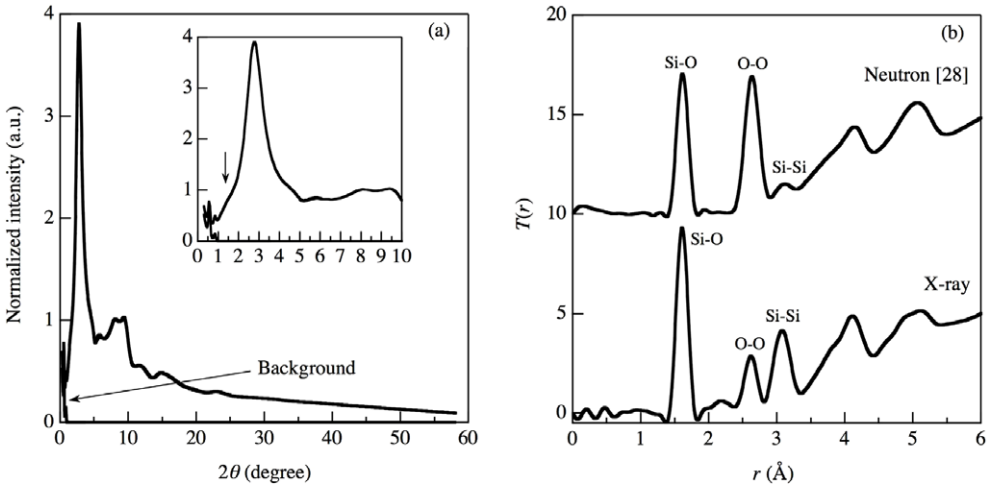

Figure 7. X-ray diffraction pattern (a), and total correlation function $T(r)$ (b) of amorphous silica. Incident energy 61.65 keV. Sample shape, flat pate of 2 mm thickness. Measured time 8.5 h. Beam size 2.5 mm (H) $\times$ 0.5 mm (W). Fourier transformation was carried out with $Q_{\max} = 30$ Å^{-1} employing the Lorch function [27].

introduction of a vacuum chamber, proper shielding around the detector with Pb, and adjusting of the incident beam stop. A relatively sharp peak observed at $2\theta = 0.5°$ arose from the scattering from the Kapton windows of the vacuum chamber. It is not necessary to measure background data at $2\theta > 1°$ when we do not use a container, because the background intensity is less than 3 cps. In addition, we can observe clearly a shoulder peak at $2\theta \sim 1.5°$ owing to the low background level. The minimum value of 2θ is 0.3°, which corresponds to $Q = 0.164$ Å^{-1}. It is possible to access a lower Q when we tune the setup of the receiving slits. The total correlation function $T(r)$ shown in figure 7(b) together with neutron data [28] has a sufficient real space resolution and very small unphysical peaks at $r < 1$ Å. Furthermore it is obvious that neutron and x-ray data exhibit different contrasts for O–O and Si–Si correlations. Recently, from reliable neutron and x-ray diffraction data, Kohara and Suzuya have succeeded in revealing differences in topological disorder [29, 30] manifested by ring statistics between amorphous silica and germania, where amorphous germania exhibits a large fraction of three-

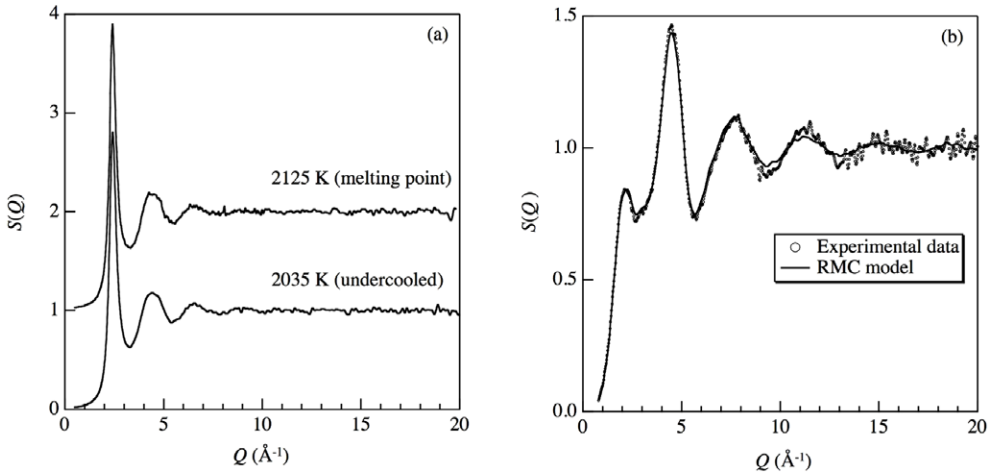

Figure 8. Total structure factors $S(Q)$ of liquid Zr [19] at 2125 and 2035 K (a) and liquid Al_2O_3 at 2400 K (b).

fold rings formed by tetrahedra [31]. Mei *et al* reported the structure of liquid silica revealed by a combination of high-energy x-rays and an aerodynamic levitation technique where a large weighting factor for the Si–Si correlation is very useful as well as the modification of the first sharp diffraction peak (FSDP) [32]. Thus, the use of the combination of neutron diffraction and high-energy x-ray diffraction as well as combination with the levitation techniques is very important for studying the structure of glass, liquid and glass formation.

3.2. Diffraction from levitated liquid

The total structure factors $S(Q)$ of liquid Zr and liquid Al_2O_3 are shown in figure 8. As can be observed in figure 8(a), the statistics of liquid Zr data are insufficient, but the diffraction data for undercooled liquid were also obtained. Furthermore, the $S(Q)$ of liquid Zr at 2125 K is consistent with published neutron diffraction data [10]. We have also succeeded in measuring the $S(Q)$ of liquid Al_2O_3 in a wide Q range as shown in figure 8(b). Our data are slightly different from that recently reported by Shankar *et al* [33], particularly in the low-Q region. In addition, the measured $S(Q)$ does not agree with the result of molecular dynamics simulation [33], however, it can well be reproduced by reverse Monte Carlo simulation (RMC) [34, 35] and is inconsistent with the structural model derived by the empirical potential structure refinement (EPSR) [36] of neutron diffraction data [13]. The detailed analysis of short- and intermediate-range structures based on the high-real space resolution data and RMC modeling is in progress. The obtained model will be the reference structure for aluminate glasses.

Although our levitation furnaces have still not made a significant contribution to the scientific field of disordered materials, the ultimate goal of studying the levitated liquid is to combine reliable diffraction data obtained in a wide Q range by the step-scan method, employing a Ge detector, and the fast diffraction measurements, using an area detector. This is the best way to obtain clues about the precise structural analysis of high-temperature liquids, that is, the determination of the structural parameters such as bond length and coordination number, which are still controversial (e.g. liquid Si) [16, 37].

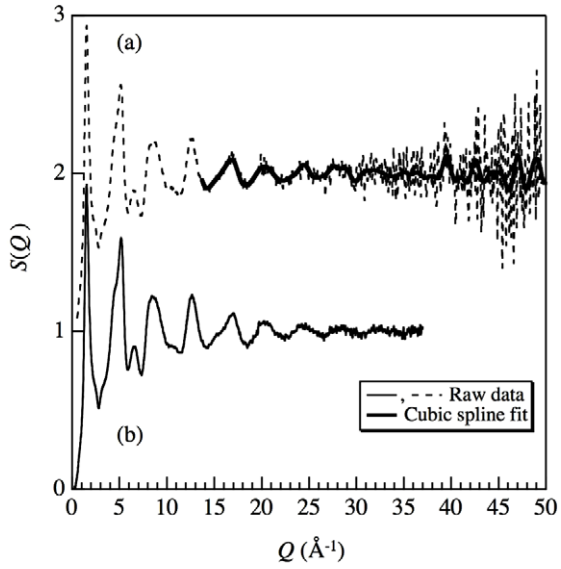

Figure 9. Total structure factors $S(Q)$ of amorphous silica: (a) BL04B2 with 61.6 keV (14 h), (b) BL08W with 176 keV (30 h).

3.3. Diffraction data obtained with 176 keV x-rays

Figure 9 shows the total structure factor $S(Q)$ of amorphous silica obtained with 176 keV x-rays at BL08W and 61.6 keV x-rays at BL04B2. We succeeded in measuring $S(Q)$ up to $Q = 37$ Å^{-1} in 14 h at BL04B2. On the other hand, although it took 30 h to obtain the structure factor up to $Q = 50$ Å^{-1} with 175.7 keV at BL08W, it was difficult to obtain sufficient statistics up to the maximum Q owing to the large contribution of incoherent scattering in the high-Q region where the contribution of coherent scattering to the total scattering intensity is very small. The diffraction patterns of liquid Hg in a 2 mm thick glass capillary and of an empty capillary are shown in figure 10(a). In the case of 176 keV, the μt of the sample is about 3.4, whereas that for 113 keV it is about 10. As can be observed in figure 10(a), the contribution of the background is successfully suppressed, and the magnitude of diffraction from the sample yields a sufficient in the low Q (if absorption is very large, the magnitude of diffraction from the sample is lower than that from the empty capillary). Figure 10(b) shows the structure factor, $S(Q)$, of liquid Hg. It took 7 h to obtain the structure factor up to $Q = 30$ Å^{-1}. As can be observed in the inset data, $S(Q)$ shows a significant oscillation up to $Q \sim 20$ Å^{-1}, where the maximum scattering angle is $\sim$13°. Thus, the use of 176 keV x-rays reduces the systematic correction terms, particularly the angle-dependent absorption correction, to a manageable level, even if the sample thickness is 2 mm. As a natural result of the small correction level, the experimental data can be well reproduced by RMC modeling up to $Q = 20$ Å^{-1}.

The pair distribution function $g(r)$ of liquid Hg is shown together with RMC data in figure 10(c). There are no bumps in the experimental $g(r)$, since we performed Fourier transformation with $Q_{\max} = 18$ Å^{-1} which can suppress termination errors in comparison with a previous synchrotron x-ray diffraction study using an energy-dispersive technique [38]. Furthermore, the asymmetrical shape of the first $g(r)$ peak can be clearly distinguished. Two coordination numbers, N_{A} and N_{B}, each with a different definition, were calculated in

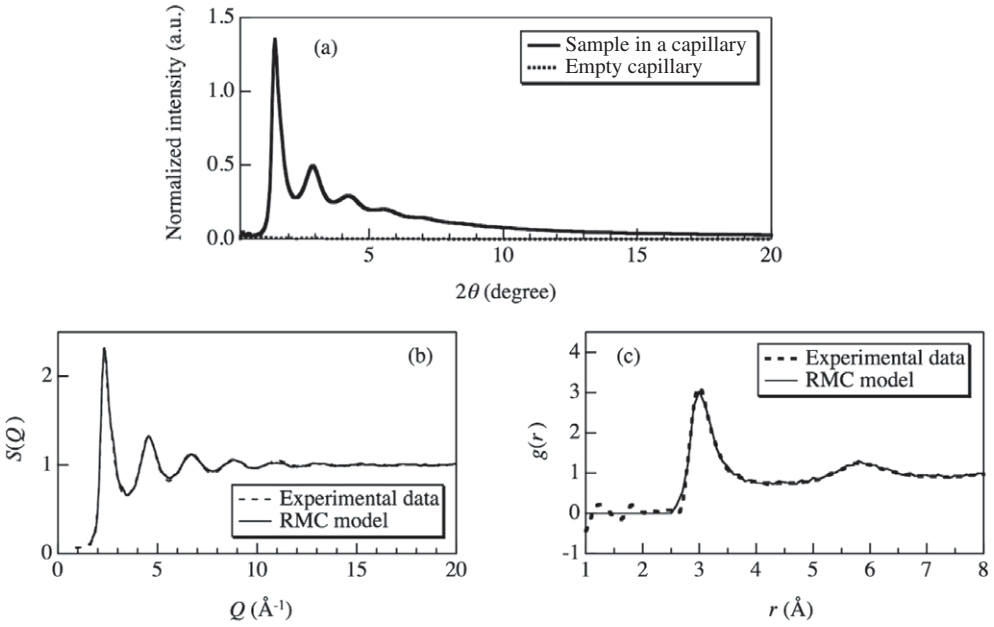

Figure 10. X-ray diffraction data for liquid Hg together with data for an empty tube (a), structure factor $S(Q)$ (b) and pair distribution function $g(r)$ (c) of liquid Hg.

accordance with the two definitions in [38] from the experimental $g(r)$ and the RMC model. Definition A involves the integration of $4\pi\rho r^2 \cdot g(r)$ up to the first maximum position of $g(r)$ (r_1) and the multiplication of the integral value by 2, where ρ denotes the average number density. Definition B involves the integration of $4\pi\rho r^2 \cdot g(r)$ up to the first minimum position of $g(r)$ ($r_{\min}(> r_1)$). The N_A and N_B are calculated to be 5.5 ($r_1 = 3.0$ Å) and 14.6 ($r_{\min} = 4.5$ Å), respectively, in good agreement with values from a previous study [38].

Figure 11 shows the typical 12-fold configuration in liquid Hg derived from the RMC snapshot. The local structure shown in figure 11 is similar to the short-range structure of α-Hg (six neighboring atoms are hexagonally arranged at 3.5 Å around a central atom and the other six atoms are located at 3.0 Å), as discussed in [38]. Thus, RMC modeling with reliable wide-Q diffraction data provides a reliable structural model for a simple liquid.

The use of 176 keV high-energy x-rays from the wiggler of SPring-8 allows us to obtain accurate diffraction data for a liquid containing heavy elements with a transmission geometry, since it reduces systematic corrections to a level which does not pose a significant problem. Furthermore, the use of a 2 mm diameter capillary as a sample container results in easier handling of liquid samples. With such advantages, the 176 keV x-rays can be used to study the structure of a metallic fluid.

3.4. High-energy x-ray diffraction under high pressure

A high-pressure x-ray diffraction study of a metallic amorphous state of SnI_4 induced by pressure was performed. SnI_4 powder was loaded to a modified Mao–Bell-type DAC. High-energy x-rays tuned to 61.6 keV were used. The diffraction pattern from amorphous SnI_4 was measured at 35, 45, 54 and 55 GPa during compression and at 25 GPa during decompression. The diffraction pattern from a non-molecular crystalline phase with a fcc structure was also

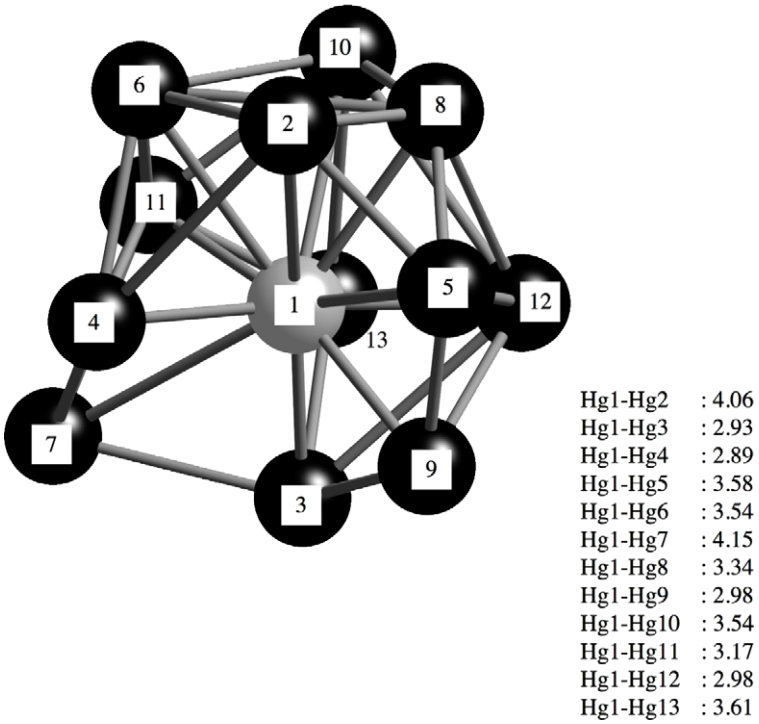

Figure 11. Typical local structure in liquid Hg obtained from RMC snapshot. Typical atomic distances are shown in Å.

measured at 65 GPa to estimate the profile of the background due to air scattering around the diffractometer and from the pressure-transmitting medium.

The total structure factors $S(Q)$ obtained at pressures between 25 and 65 GPa [39] are shown in figure 12, together with data of liquid measured at 160 °C with 113 keV x-rays [40]. The FSDP observed at $Q \sim 2.4$ Å^{-1} at 25 GPa is intense and the second peak overlaps the third one. Such features are commonly found in $S(Q)$ for pure metallic glasses of Ni and Fe at ambient pressure [41], but not in $S(Q)$ for molecular liquids as shown in figure 12. The FSDP shifts position to a higher Q and increases in peak height with increasing pressure. A detailed structural investigation is in progress using RMC simulation in comparison with molecular liquid data.

The combination of high-energy x-rays and a DAC system is one of the most powerful tools for studying structural modification in disordered materials under high pressures.

4. Conclusion

We introduced high-energy x-ray diffraction beamlines and a dedicated diffractometer for glass, liquid and amorphous materials at SPring-8 and reported the recent development of ancillary equipment: automatic sample changer, conventional high-temperature furnace and levitation furnace. We also presented the diffraction data obtained under high pressures and the advantages of using 176 keV high-energy x-rays. Though recent scientific topics are not introduced in this paper, high-energy diffraction beamline BL04B2 is found to play an important role in contributing to scientific research on structurally disordered materials by

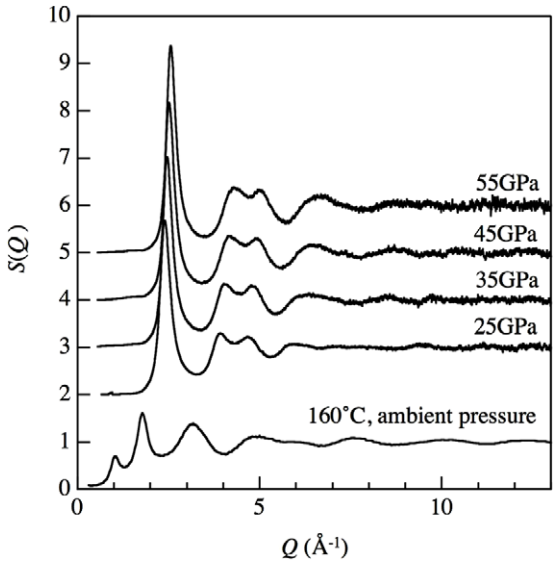

Figure 12. Total structure factors $S(Q)$ of SnI_4 at 25, 35, 45 and 55 GPa [39] during decompression together with liquid data obtained at ambient pressure (160 °C) [40].

studies, for example, on nanometer-sized silica particles [42], an unusual network structure in forsterite glass [43], isotopic quantum effects in water [44], a fast phase change in the mother material of a DVD-RAM (digital versatile disk-random access memory) [45] and the structural analysis of AsS bulk glass synthesized from a high-pressure melt [46].

The techniques used in x-ray diffraction experiments under extreme conditions have been well developed and the combined use of neutron diffraction and high-energy x-ray diffraction has become very popular. On the other hand, the activity of anomalous x-ray scattering (AXS) is still not widely used owing to difficulties in both the experiments and the data analysis, although AXS is shown to be a powerful technique for structural study in disordered materials. Therefore, our next target is the development of a dedicated beamline and diffractometer for AXS to study the structures of disordered materials.

Acknowledgments

We appreciate Drs A Mizuno, T Masaki, T Ishikawa and Professor M Watanabe for their significant contributions to the development of levitation furnaces. We thank Professor N Hamaya and Dr A Ohmura for developing techniques for use in high-pressure experiments on disordered materials. Discussion with Dr J K R Weber is gratefully appreciated. This work was financially supported by a Grant in Aid for Scientific Research by the Japan Society for the Promotion of Science.

References

[1] Neuefeind J and Poulsen H F 1995 *Phys. Scr.* **T57** 112
[2] Poulsen H F, Neuefeind J, Neumann H-B, Schneider J R and Zeidler M D 1995 *J. Non-Cryst. Solids* **188** 63
[3] Fischer H E, Barnes A C and Salmon P S 2006 *Rep. Prog. Phys.* **69** 233

[4] Egami T and Billinge S J L 2003 *Underneath the Bragg Peaks: Structural Analysis of Complex Materials* (Amsterdam: Pergamon)
[5] Isshiki M, Ohishi Y, Goto S, Takeshita K and Ishikawa T 2001 *Nucl. Instrum. Methods* A **467/468** 663
[6] Tanaka H *et al* 2006 *J. Synchrotron Radiat.* **13** 378
[7] Kohara S, Suzuya K, Kashihara Y, Matsumoto N, Umesaki N and Sakai I 2001 *Nucl. Instrum. Methods* A **467/468** 1030
[8] Notthoff C, Franz H, Hanfland M, Herlach D M, Holland-Moritz D and Petry W 2000 *Rev. Sci. Instrum.* **71** 3791
[9] Holland-Moritz D, Schenk T, Convert P, Hansen T and Herlach D M 2005 *Meas. Sci. Technol.* **16** 372
[10] Schenk T, Holland-Moritz D, Simonet V, Bellissent R and Herlach D M 2005 *Phys. Rev. Lett.* **89** 075507
[11] Krishnan S and Price D L 2000 *J. Phys.: Condens. Matter* **12** R145
[12] Landron C, Hennet L, Coutures J P, Jenkins T E, Alétru C, Greaves G N, Soper A K and Derbyshire G 2000 *Rev. Sci. Instrum.* **71** 1745
[13] Landron C, Hennet L, Jenkins T E, Greaves G N, Coutures J P and Soper A K 2001 *Phys. Rev. Lett.* **86** 4839
[14] Kimura H, Watanabe M, Izumi K, Hibiya T, Holland-Moritz D, Schenk T, Bauchspiß K R, Schneider S, Egry I, Funakoshi K and Hanfland M 2001 *Appl. Phys. Lett.* **78** 604
[15] Kelton K F, Lee G W, Gangopadhyay A K, Hyers R W, Rathz T J, Rogers J R, Robinson M B and Robinson D S 2003 *Phys. Rev. Lett.* **90** 195504
[16] Kim T H, Lee G W, Sieve B, Gangopadhyay A K, Hyers R W, Rathz T J, Rogers J R, Robinson D S, Kelton K F and Goldman A I 2005 *Phys. Rev. Lett.* **95** 085501
[17] Gangopadhyay A K, Lee G W, Kelton K F, Rogers J R, Goldman A I, Robinson D S, Rathz T J and Hyers R W 2005 *Rev. Sci. Instrum.* **76** 073901
[18] Mizuno A, Matsumura S, Watanabe M, Kohara S and Takata M 2005 *Mater. Trans.* **46** 2899
[19] Masaki T, Ishikawa T, Paradis P-F, Yoda S, Okada J T, Watanabe Y, Nanao S, Ishikura A, Higuchi K, Mizuno A, Watanabe M and Kohara S 2007 *Rev. Sci. Instrum.* **89** 026102
[20] Sakurai Y 1998 *J. Synchrotron Radiat.* **5** 208
[21] Baron A Q R, Tanaka Y, Goto S, Takeshita K, Matsushita T and Ishikawa T 2000 *J. Phys. Chem. Solids* **61** 461
[22] Baron A Q R, Tanaka Y, Miwa D, Ishikawa D, Mochizuki T, Takeshita K, Goto S, Matsushita T and Ishikawa T 2001 *Nucl. Instrum. Methods* A **467/468** 627
[23] Marechal X-M, Hara T, Tanabe T, Tanaka T and Kitamura H 1998 *J. Synchrotron Radiat.* **5** 431
[24] Yamaoka H, Hiraoka N, Itou M, Mizumaki M, Sakurai Y, Kakutani Y, Koizumi A, Sakai N and Higashi Y 2000 *J. Synchrotron Radiat.* **7** 69
[25] Mozzi R L and Warren B E 1969 *J. Appl. Crystallogr.* **2** 164
[26] Wright A C 1994 *J. Non-Cryst. Solids* **179** 84
[27] Lorch E A 1969 *J. Phys. C: Solid State Phys.* **2** 229
[28] http://www.isis.rl.ac.uk/disordered/Database/DBMain.htm
[29] Cooper A R 1978 *Phys. Chem. Chem. Glasses* **19** 60
[30] Gupta P K and Cooper A R 1990 *J. Non-cryst. Solids* **123** 14
[31] Kohara S and Suzuya K 2005 *J. Phys.: Condens. Matter* **17** S17
[32] Mei Q, Benmore C J and Weber J K R 2007 *Phys. Rev. Lett.* **98** 057802
[33] Krishnan S, Hennet L, Jahn S, Key T S, Madden P A, Saboungi M L and Price D L 2005 *Chem. Mater.* **17** 2662
[34] McGreevy R L and Pusztai L 1988 *Mol. Simul.* **1** 359
[35] McGreevy R L 2001 *J. Phys.: Condens. Matter* **13** R877
[36] Soper A K 2005 *Phys. Rev.* B **72** 104204
[37] Jakse N, Hennet L, Price D L, Krishnan S, Key T S, Artacho E, Glorieux B, Pasturel A and Saboungi M L 2003 *Appl. Phys. Lett.* **83** 4734
[38] Inui M, Hong X and Tamura K 2003 *Phys. Rev.* B **68** 094108
[39] Ohmura A, Hamaya N, Sato K, Ogawa C, Isshiki M and Ohishi Y 2002 *J. Phys.: Condens. Matter* **14** 10553
[40] Fuchizaki K, Kohara S, Ohishi Y and Hamaya N 2007 *J. Chem. Phys.* **127** 064504
[41] Ichikawa T 1975 *Phys. Status Solidi* a **29** 293
[42] Uchino T, Aboshi T, Kohara S, Ohishi Y, Sakashita M and Aoki K 2004 *Phys. Rev.* B **69** 155409
[43] Kohara S, Suzuya K, Takeuchi K, Loong C-K, Grimsditch M, Weber J K, Tangeman J A and Key T S 2004 *Science* **303** 1649
[44] Hart R T, Benmore C J, Neuefeind J, Kohara S, Tomberli B and Egelstaff P A 2005 *Phys. Rev. Lett.* **94** 047801
[45] Kohara S, Kato K, Kimura S, Tanaka H, Usuki T, Suzuya K, Tanaka H, Moritomo Y, Matsunaga T, Yamada N, Tanaka Y, Suematsu H and Takata M 2006 *Appl. Phys. Lett.* **89** 201910
[46] Brazhkin V V, Gavrilyuk A G, Lyapin A G, Timofeev Y A, Katayama Y and Kohara S 2007 *Appl. Phys. Lett.* **91** 031912